

# Nogo-A is secreted in extracellular vesicles, occurs in blood and can influence vascular permeability

Journal of Cerebral Blood Flow & Metabolism  
2024, Vol. 44(6) 938–954  
© The Author(s) 2023



Article reuse guidelines:  
sagepub.com/journals-permissions  
DOI: 10.1177/0271678X231216270  
journals.sagepub.com/home/jcbfm



Ruslan Rust<sup>1,2,3,\*,#</sup> , Mea M Holm<sup>1,2,\*</sup>, Matteo Egger<sup>2</sup>, Oliver Weinmann<sup>1</sup>, Daniëlle van Rossum<sup>4</sup>, Fruzsina R Walter<sup>5</sup>, Ana Raquel Santa-Maria<sup>5,†</sup>, Lisa Grönnert<sup>1</sup>, Michael A Maurer<sup>1</sup> , Simon Kraler<sup>6</sup>, Alexander Akhmedov<sup>6</sup> , Rose Cideciyan<sup>6</sup>, Thomas F Lüscher<sup>6,7</sup>, Maria A Deli<sup>5</sup>, Inge K Herrmann<sup>8,9</sup> and Martin E Schwab<sup>1,2,3</sup>

## Abstract

Nogo-A is a transmembrane protein with multiple functions in the central nervous system (CNS), including restriction of neurite growth and synaptic plasticity. Thus far, Nogo-A has been predominantly considered a cell contact-dependent ligand signaling via cell surface receptors. Here, we show that Nogo-A can be secreted by cultured cells of neuronal and glial origin in association with extracellular vesicles (EVs). Neuron- and oligodendrocyte-derived Nogo-A containing EVs inhibited fibroblast spreading, and this effect was partially reversed by Nogo-A receptor SIPR2 blockage. EVs purified from HEK cells only inhibited fibroblast spreading upon Nogo-A over-expression. Nogo-A-containing EVs were found *in vivo* in the blood of healthy mice and rats, as well as in human plasma. Blood Nogo-A concentrations were elevated after acute stroke lesions in mice and rats. Nogo-A active peptides decreased barrier integrity in an *in vitro* blood-brain barrier model. Stroked mice showed increased dye permeability in peripheral organs when tested 2 weeks after injury. In the Miles assay, an *in vivo* test to assess leakage of the skin vasculature, a Nogo-A active peptide increased dye permeability. These findings suggest that blood borne, possibly EV-associated Nogo-A could exert long-range regulatory actions on vascular permeability.

## Keywords

Nogo-A, SIPR2, exosomes, stroke, blood-brain barrier, leakage

Received 26 May 2023; Revised 10 October 2023; Accepted 20 October 2023

## Introduction

Nogo-A is a membrane protein enriched in oligodendrocytes, CNS myelin and subtypes of neurons that exerts repulsive and inhibitory effects on growing neurites and vascular tip cells during development, and is

<sup>7</sup>Royal Brompton and Harefield Hospitals and Imperial College, London, United Kingdom

<sup>8</sup>Particles Biology Interactions Laboratory, Swiss Federal Laboratories for Materials Science and Technology (Empa), St. Gallen, Switzerland

<sup>9</sup>Nanoparticle Systems Engineering Laboratory, Department of Mechanical and Process Engineering, ETH Zurich, Zurich, Switzerland

\*Both authors contributed equally.

<sup>#</sup>Current address: Department of Physiology and Neuroscience Keck School of Medicine of the University of Southern California, Los Angeles, USA

<sup>†</sup>Current address: Wyss Institute for Biologically Inspired Engineering at Harvard University, Boston, USA

## Corresponding author:

Martin E Schwab, Institute for Regenerative Medicine (IREM), University of Zurich, Wagistrasse 12, CH-8952 Schlieren, Switzerland.  
Email: schwab@irem.uzh.ch

<sup>1</sup>Brain Research Institute, University of Zürich, Switzerland

<sup>2</sup>Department of Health Sciences and Technology, ETH Zürich, Switzerland

<sup>3</sup>Institute for Regenerative Medicine (IREM), University of Zurich, Switzerland

<sup>4</sup>Department of Translational Neuroscience, UMC Utrecht, Netherlands

<sup>5</sup>Biological Barriers Research Group, ELKH Biological Research Centre, Szeged, Hungary

<sup>6</sup>Center for Molecular Cardiology, University of Zurich, Switzerland

an important restricting factor for structural and synaptic plasticity and axonal as well as vascular regeneration after CNS injuries.<sup>1-4</sup> With two long hydrophobic sequences at its C-terminus, Nogo-A was primarily seen as a contact-dependent ligand interacting with membrane-bound receptor complexes, whereby two different sequences of the ligand Nogo-A interact with two different binding partners and their associated components.<sup>5-7</sup> The Nogo-66 region binds receptors called NgR1 and PirB with the co-receptor components p75 or Troy and LINGO-1 or AMIGO-3.<sup>1,8</sup> The more N-terminal Nogo-A- $\Delta$ 20 region binds to either a complex of the G-protein coupled receptor S1PR2 with the tetraspanin TSPAN3 and/or the recently identified Nogo-A- $\Delta$ 20 interaction partners heparan sulfate proteoglycans (HSPGs) syndecan-3/4.<sup>9-11</sup> Signalling via both Nogo-66 and Nogo-A- $\Delta$ 20 leads to Rho-A activation and actin cytoskeleton modification; Nogo-A- $\Delta$ 20 has been suggested to also affect gene expression.<sup>2,9,12</sup> However, it remains unknown whether Nogo-A always acts as a full-length ligand, or whether the hydrophilic, approximately 1000 aa long N-terminus is proteolytically processed to release an active fragment as a soluble ligand with further biological functions. Although proteolytic processing of N-terminal Nogo-A has been described previously, this observation was linked to Nogo-A inactivation rather than to active fragment release.<sup>13</sup> Hence, the available evidence is consistent with the concept that full-length Nogo-A acts as a membrane-bound, cell contact-dependent ligand via engaging Nogo receptors on adjacent cells. Only recently, first evidence arose that Nogo-A proteolytic fragments can be released via extracellular vehicles (EVs) to act as a diffusible inhibitor of neurite outgrowth.<sup>14</sup>

EVs are nano-to-micrometer sized cell-derived vesicles carrying various nucleic acids, soluble proteins and transmembrane proteins.<sup>15</sup> In recent years, EVs have emerged as important multi-modal signalling vehicles also in the CNS (patho-)biology. Neuronal activity leads to an increase in EV secretion by both neuronal and glial cells, and these EVs can influence neuronal excitability.<sup>16-19</sup> Oligodendroglial EVs have been shown play neuro-protective roles under conditions of ischemia,<sup>20</sup> and Schwann cell EVs can increase regrowth of neurites after injury in the peripheral nervous system (PNS).<sup>21</sup> EVs may also be involved in carrying morphogens across synapses and potentially to distant sites, as Wnt-carrying EVs are secreted by various cell types and have been shown to be functionally relevant for the coordinated growth of muscle and synapse at *Drosophila* neuromuscular junctions (NMJ).<sup>22,23</sup>

Here, we report that full-length and bioactive Nogo-A is sorted into EVs and can cause spreading inhibition

of fibroblasts via S1PR2 signaling *in vitro*. EVs containing Nogo-A were recovered from blood of healthy rodents and humans; blood Nogo-A levels were elevated in stroked mice and rats, demonstrating that EVs containing Nogo-A are present under physiological conditions and react to pathological conditions. The active Nogo-A fragment D20 increased brain endothelial cell permeability in an *in vitro* blood-brain barrier (BBB) model. Injections of this peptide also increased vascular permeability in the Miles assay, an *in vivo* assay for skin vessel permeability. Mice with cortical strokes, which had high levels of blood Nogo-A, showed higher vessel permeability in several of their organs.

## Materials & methods

### Antibodies and reagents

For western blotting, the following primary antibodies were used at the indicated concentrations: 0.2  $\mu$ g/ml mouse anti-Alix clone 3A9 (Cell Signaling Technology, 21715), 0.25-0.5  $\mu$ g/ml mouse anti-Alix clone 49 (BD Biosciences, 611620), 0.25-0.5  $\mu$ g/ml mouse anti-flotillin1 clone 18 (BD Biosciences, 610820), 0.06  $\mu$ g/ml human anti-CD63 clone REA563 (Miltenyi Biotech, 130108892), 0.5  $\mu$ g/ml mouse anti-CD9 clone H19a (Biolegend, 312102), 1  $\mu$ g/ml rabbit anti-Ago2 (Abcam, ab32381), 0.12  $\mu$ g/ml rabbit anti-GM130 EP892Y (Abcam, ab52649), 1  $\mu$ g/ml rabbit anti-Calnexin (Abcam, ab22595), 3.9  $\mu$ g/ml mouse anti-flag M2 (Sigma, F3165), 0.2  $\mu$ g/ml mouse anti-GAPDH clone 6C5 (Abcam, ab8245), 1:10000-1:20000 rabbit anti-Nogo serum Rb1 (produced in house,<sup>24,25</sup> 0.75  $\mu$ g/ml mouse anti-Nogo-A 11C7 (produced in house.<sup>24</sup> Secondary HRP-coupled antibodies were all purchased from Thermo Fisher Scientific and used at a concentration of 0.05-0.1  $\mu$ g/ml. For TEM with immunogold labeling, the following primary antibodies were used at the indicated concentrations: 1:40 anti-Nogo-A Rb172A serum (produced in house,<sup>24,25</sup> 1:40 control rabbit pre-immunisation serum (produced in house,<sup>24</sup> 10  $\mu$ g/ml human anti-CD63 clone REA563 (Miltenyi Biotech, 130108892), 156  $\mu$ g/ml mouse anti-flag M2 (Sigma, F3165). Secondary antibodies or protein A conjugated to 10 nm gold particles were obtained from British BioCell and used at a dilution of 1:25. For immunocytochemistry, the following primary antibodies were used at the indicated concentrations: 1  $\mu$ g/ml mouse anti- $\beta$ 3-tubulin (Promega, G712A), 2  $\mu$ g/ml mouse anti-RhoA-GTP (New East Biosciences, 26904). As secondary antibodies, 1  $\mu$ g/ml anti-mouse Cy3-coupled antibodies (Invitrogen, A10521) were used. 1:200 Phalloidin Alexa Fluor 488 (Invitrogen, A12379) was used to stain the

cytoskeleton, and 50 nM DAPI (Invitrogen, D3571) was used as nuclear counterstain. For spreading assays, JTE-013 was purchased from Tocris and used at a final concentration of 10  $\mu$ M. The ROCK inhibitor Y-27632 was purchased from Sigma and used at a final concentration of 1–10  $\mu$ M.

### Plasmids & cloning

Cloning of Flash-Flag double tagged constructs of Nogo-A was performed using the general method originally described by.<sup>26</sup> Briefly, the sequences of Nogo-A flanking the desired tag insertion site both N-terminally and C-terminally were amplified out of the full-length mouse Nogo-A sequence through polymerase chain reaction (PCR) with the primers listed in Suppl. Table 2 using the KAPA HiFi HotStart PCR Kit (Roche). The vector AbVec-hIgG1 (FJ475055) was digested with the restriction enzymes HindIII (New England Biosciences, R0104S) and EcoRI (New England Biosciences, R0101S) to remove the IgG sequence and linearize the vector. The digested vector and the Nogo-A PCR products (insert) were then ligated with the Gibson Assembly<sup>®</sup> Master Mix (New England Biosciences) according to the manufacturer's instructions. Briefly, the molar vector to insert ratios were chosen depending on the size of the insert (total of 0.02–0.5 pmol DNA), mixed in a final volume of 10  $\mu$ l of water, added to 10  $\mu$ l of Gibson assembly master mix, and incubated for 15 minutes at 50 °C. Immediately after the ligation, the assembled product was transformed into TOP10 chemically competent *E. coli* through heat shock (42 °C for 30 sec). Transformed bacteria were plated on Agar in the presence of 100  $\mu$ g/ml ampicillin (Sigma Aldrich) for 16 h, followed by colony picking, liquid culture, and purification of the DNA constructs through QIAprep Spin Miniprep Kit (Qiagen) according to the manufacturer's instructions. Proper insertion of the tag (5'-TGT TGT CCA GGC TGT TGT GGA AGC GAC TAC AAA GAC GAT GAC GAC AAG-3') was confirmed through sequencing.

### Cell culture

Neuro-2a (N2a), HEK-293T, N1E-115, and Swiss 3T3 cells were obtained from ATCC and maintained at 37 °C in a humidified atmosphere with 5% CO<sub>2</sub>, in Dulbecco's Modified Eagle Medium (DMEM) supplemented with 10% fetal bovine serum (FBS). The oligodendrocyte precursor cell line Oli-neu was a kind gift from Dr. Jacqueline Trotter (University of Mainz, Germany). Oli-neu cells were maintained in a humidified atmosphere at 37 °C and 8% CO<sub>2</sub>, in SATO medium supplemented with 1% horse serum, 10 ng/ml PDGF

(Peprotech) and 10 ng/ml FGF (Peprotech). For EV isolation, cells were plated sub-confluent (60–70%) in 15 cm dishes (TPP) in full growth medium for 16 h. The cells were then washed twice in phosphate buffered saline (PBS) in quick succession, and once in EV harvesting medium for 15 min under normal culture conditions, followed by incubation in 15 ml EV harvesting medium for 24 h or 48 h. For N2a and HEK-293T, serum-free OptiMem<sup>™</sup> (Invitrogen) was used as EV harvesting medium. For Oli-neu, serum-free SATO supplemented with FGF and PDGF was used as the EV harvesting medium.

### EV isolation through ultracentrifugation

The EV harvesting medium, i.e. conditioned culture medium (CCM), was subjected to differential centrifugation as described previously,<sup>27</sup> with minor modifications. Briefly, the CCM was pre-cleared through sequential centrifugation at 300 g for 5 min, 2000 g for 20 min, and 10 000 g for 30 min. The pre-cleared CCM was then subjected to ultracentrifugation at 100 000 g for 70 min in an SW28 rotor (Beckmann). Where stated, the supernatant was collected and concentrated 100-fold in Amicon Ultra centrifugal ultrafiltration devices with 10 kDa cut-off (Millipore), according to the manufacturer's instructions. The pellets from the 100 000 g ultracentrifugation, containing the EVs, were re-suspended in 500  $\mu$ l PBS and pooled in a final volume of 13 ml PBS. For morphology analysis through TEM, the EVs were fixed at this stage with a final w/v of 0.4% paraformaldehyde (PFA). The EVs were then subjected to a second round of ultracentrifugation at 100 000 g for 70 min in a TH-641 rotor (Sorvall). The supernatant was discarded, and the final pellet was re-suspended in 50–150  $\mu$ l PBS (for TEM and functional assays) or RIPA buffer (for western blotting). All centrifugation steps were performed at 4 °C. The ultracentrifugation-based EV isolation protocol was used for all functional assays (Figures 3 and 4). This protocol was optimized for functionality and morphological integrity of EVs, ensuring that the EVs used in the functional assays were of the highest quality.

### EV isolation through density gradient and ultracentrifugation for extended characterization

Discontinuous iodixanol density gradients were prepared as described previously<sup>28</sup> with some minor modifications. Briefly, a working solution (WS) of iodixanol was prepared by mixing 60% iodixanol (OptiPrep<sup>™</sup>, Axis Shield) with a working buffer (WB) (0.25 M sucrose, 6 mM EDTA, 60 mM Tris-HCl, pH 7.4). Appropriate amounts of WS were then

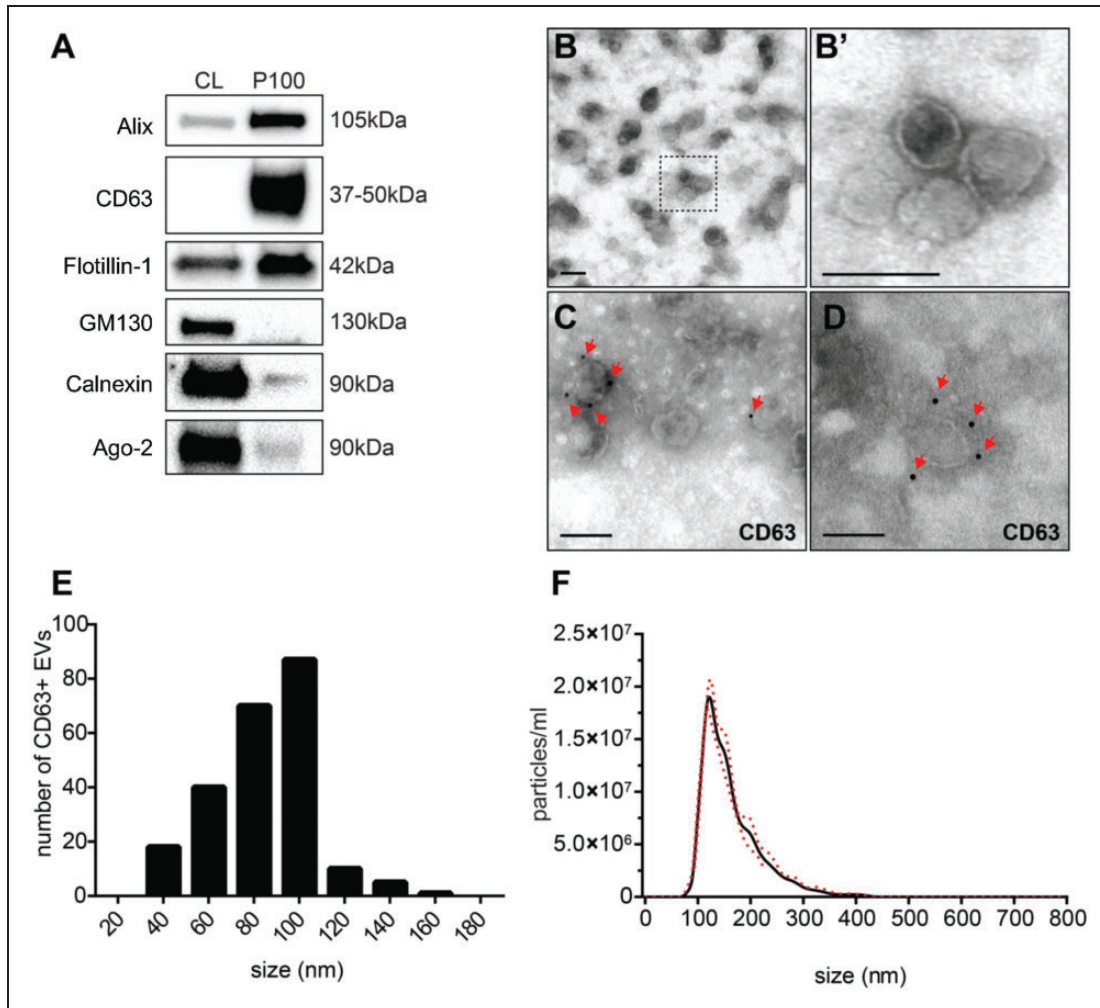


**Figure 1.** Validation of EV isolation. EVs were isolated from pre-cleared cell culture supernatants through two rounds of ultracentrifugation at 100 000 g for 70 min and re-suspended in PBS for analysis. (a) Representative Western blots for EV marker proteins (Alix, CD63, Flotillin-2), and proteins used as negative controls (Calnexin, GM130, Ago2). Similar results were observed in >3 independent experiments. (b and b') Representative TEM images showing the morphology of the isolated EVs. (b') is cropped and magnified from the region in (b) indicated by the dotted line. (c) and (d) Representative TEM images of EVs with immuno-gold labelling for CD63. Red Arrows indicate positive labeling. Scale bars = 100nm in all TEM images. (e) Size distribution of immune-gold (CD63<sup>+</sup>) labelled EVs from TEM analysis from n = 3 independent EV isolations. (f) Representative size distribution of the isolated EVs from NTA. Red dotted line represents the standard deviation from 3 independent measurements. – CL= ultracentrifugation supernatant; P100= pellet of 100 000 g centrifugation.

mixed with a homogenization medium (0.25 M sucrose, 1 mM EDTA, 10 mM Tris-HCL, pH 7.4) to obtain solutions containing 5%, 10%, 20%, and 40% iodixanol. The gradient was then prepared in a 4.9 ml polyallomere ultracentrifugation tube (Beckmann) by layering 1.2 ml of each of the 5%–40% iodixanol solutions, starting with the 40% solution at the bottom of the tube. The EV containing sample, prepared through pre-clearing as described above and concentrated 50–100× in Amicon Ultra devices with 10 kDa cut-off (Millipore), was then layered on top of the 5% fraction. The gradients were centrifuged at 100 000 g for 18 h at

4 °C in an SW40.1Ti rotor (Beckmann), and 10 fractions of 500 µl were collected from the top. The fractions were diluted 1:10 in PBS, and concentrated to 50 µl in Amicon Ultra devices with 30 kDa cut-off (Millipore). Samples were stored at –80 °C until further processing. The density gradient ultracentrifugation protocol was used to isolate EVs for extended protein characterization (Figures 1 and 2). This protocol was optimized to separate the different fractions of EVs during isolation, allowing for a more detailed understanding of the protein composition of each fraction.

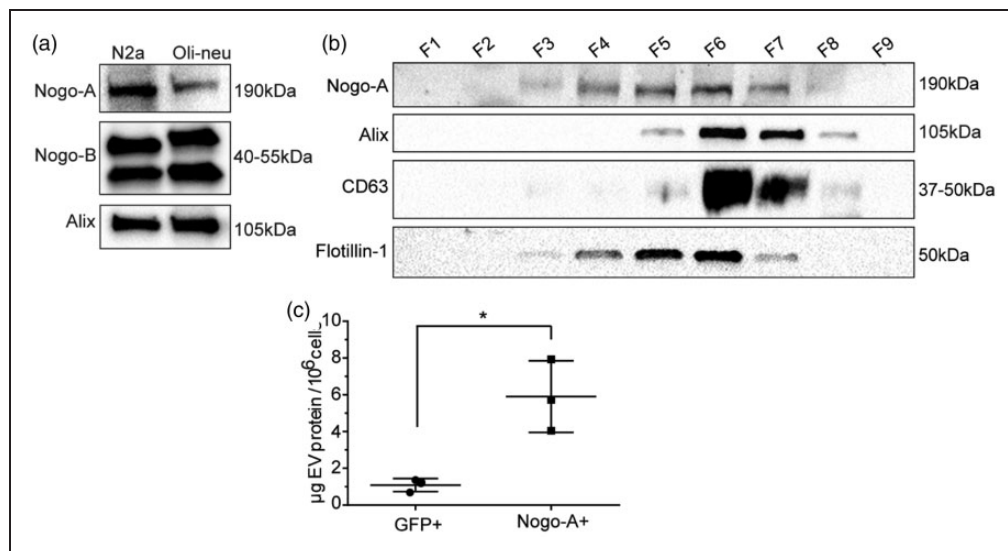


**Figure 2.** Nogo-A is present in extracellular vesicles (EVs). (a) Representative western blots of EVs from N2a and Oli-Neu cells, pelleted through ultracentrifugation. Detection of Nogo-A/-B was performed with the Rb172A serum. (b) Density gradient fractionation of the supernatant of N2a cells. F1 = top fraction, F10 = bottom fraction (not shown). Note the overlap in fractions positive for Nogo-A and Flotillin-1 (F4-F7). (c) Quantification of the total yield of EVs per  $10^6$  secreting cells, measured as  $\mu\text{g}$  of EV protein. Statistical test performed was an unpaired student's t-test,  $n = 3$ ,  $p = 0.013$ .

### Animals

All animal experiments were approved by the Cantonal Veterinary Department of Zurich. Experiments were conformed to the guidelines of the Swiss Animal Protection Law, Veterinary Office, Canton of Zurich (Act of Animal Protection December 16, 2005, and Animal Protection Ordinance April 23, 2008, animal welfare assurance number ZH231/2018). Data were reported according to the ARRIVE guidelines. Adult female wildtype mice (10–14 weeks) of the C57BL/6 strain (19–25 g) were used. Mice were housed in standard Type II/III cages at least in pairs in a temperature and humidity-controlled room with a constant 12/12 h light/dark cycle (light on from 6:00 a.m. until 6:00 p.m.).

### Photothrombotic stroke

Animals were deeply anesthetized with 5% isoflurane (Attane, Provet AG) in a transparent induction chamber. Stroke surgery was performed under 1.5–2% isoflurane. A photothrombotic stroke to unilaterally lesion the sensorimotor cortex was induced on the right hemisphere, as previously described.<sup>3,29–31</sup> Briefly, animals were fixed in a stereotactic frame (David Kopf Instruments) and the skull was exposed through a midline skin incision. A cold light source (Olympus KL 1500LCS, 150 W, 3000 K) was positioned over the right forebrain cortex at anterior/posterior:  $-1.5 \text{ mm}$  to  $+1.5 \text{ mm}$  and medial/lateral  $0 \text{ mm}$  to  $+2 \text{ mm}$  relative to Bregma. Rose Bengal (10 mg/ml,

in 0.9% NaCl, Sigma) was injected intraperitoneally 5 minutes prior to illumination. Subsequently, the exposed area was illuminated through the intact skull. After 10.5 minutes of illumination, light exposure was stopped. For postoperative care, all animals received analgesics (Novalgine, Sanofi) for at least 3 days after surgery.

### Human samples

20 ml of venous blood was drawn from healthy subjects (Blood Donation Center Zurich, Zurich, Switzerland) using EDTA tubes and centrifuged at 2000xrcf at  $4^\circ\text{C}$  for 15 minutes before fully anonymized plasma samples were stored at  $-80^\circ\text{C}$ . Healthy study participants were recruited within the framework of the SPUM-ACS study, as reported<sup>32</sup> and all participants gave informed consent prior to their enrolment. This study was conducted according to the declaration of Helsinki and was approved by the institutional review board (Cantonal Ethics Committee Zurich, Switzerland; reference number: EK-1688/2019-01809).

### Graphs and statistical tests

All graphs and statistical analyses were computed in GraphPad Prism version 7.03. Unpaired student's t-tests were used to compare two groups, and a one-way ANOVA with Bonferroni multiple comparisons test was used to compare multiple groups.

**Please find more details to methods in the Supplementary material.**

## Results

### *Nogo-A is associated with extracellular vesicles secreted in vitro*

First, we isolated EVs from culture supernatants of N2a neuroblastoma cells known to contain Nogo-A through ultracentrifugation as described previously.<sup>27</sup> The resultant EV preparation was characterized according to the recommendations of the international Society of extracellular vesicles (ISEV).<sup>33</sup> Through Western blotting, we confirmed the enrichment of the EV-associated marker proteins Alix, CD63 and Flotillin-2 in the EV pellet (Figure 1(a)). The absence of significant under-representation of the Golgi-associated protein GM130 and the endoplasmic reticulum (ER)-associated protein Calnexin indicated that the EV preparation was not contaminated by either intracellular proteins or apoptotic bodies (Figure 1(a)). A very low level of contamination from soluble proteins co-pelleting with the EVs was detected using Ago-2 as a surrogate marker, as previously described<sup>28</sup> (Figure 1(a)). Particles with a morphology characteristic for extracellular vesicles, a visible membrane bilayer, and positive labelling for CD63 were observed through transmission electron microscopy (TEM) (Figure 1(b) to (d)). The size of the CD63<sup>+</sup> vesicles ranged from 40-160nm in diameter, corresponding to the size range expected for endosome-derived exosomes (Figure 1(e)). Through nanoparticle tracking (NTA), we confirmed that the population of particles as a whole had a hydrodynamic diameter with a peak at 100 nm (Figure 1(f)), in line with characteristics of EVs<sup>34-36</sup> and showed high consistency between the different EV isolations.

We then applied this isolation method to the detection of Nogo-A in EV pellets from N2a cells and the oligodendrocyte precursor cell line Oli-neu. Through Western blotting with an antibody against Nogo-A/-B (Rb172A),<sup>24</sup> we identified both Nogo-A and -B in EV pellets from the cell lines (Figure 2(a)). These data suggested that Nogo-A could be secreted in association with EVs, or it could be co-pelleting with the EVs in an unspecific manner. To determine whether Nogo-A was specifically associated with the EV fraction, we carried out density gradient fractionation of cell culture supernatants. Nogo-A was present in fractions positive for Alix, CD63 and Flotillin-1, and absent from other fractions (Figure 2(b)). Interestingly, Nogo-A+ fractions overlapped perfectly with Flotillin-1+ fractions, while Alix+ and CD63+ fractions were only partially overlapping with the Nogo-A+/Flotillin-1+ fraction. This result led us to conclude that Nogo-A may be specifically associated with a Flotillin-1+ subpopulation of EVs. Next, we assessed whether

over-expression of Nogo-A in HEK cells, a cell line that does not normally express Nogo-A<sup>37</sup> (Suppl. Fig. 1), would lead to its secretion in EVs. We observed a 8-fold upregulation in the total amount of EVs secreted by Nogo-A+ cells relative to GFP+ cells (Figure 2(c)). Taken together, these results suggest that Nogo-A over-expression in HEK cells may lead to an increased secretion of a specific subtype of EV negative for Alix, and positive for Flotillin-1 and GAPDH.

### *Nogo-A is associated with the EV membrane with the N-terminus facing out*

For EV-associated Nogo-A to be functional as a signalling ligand, the N-terminal Nogo-A- $\Delta$ 20 and/or the Nogo-66 region would be expected to face the extracellular space, as has been shown for plasma membrane-associated Nogo-A.<sup>24,25,38</sup> To investigate this, we carried out TEM imaging of EVs with immunogold labelling for the N-terminus of Nogo-A. We found that the Nogo-A antibodies labelled the membrane of 8% of the EVs on average, while a control IgG did not label any EVs (Suppl. Fig. 2A-C, E). The relative labelling index (RLI) of 1.9 and Chi square ( $\chi^2$ ) value of 94.8 indicated that the gold labels were preferentially associated with the EV membrane ( $p < 0.001$ , Suppl. Table 1). The number of gold dots per EV appeared to be increased upon transgenic over-expression of Nogo-A (Suppl. Fig. 2D). For purposes of comparison, we also quantified the labelling for the EV surface marker CD63 and found that 23% of the EVs secreted by N2A neuroblastoma cells were labelled (Suppl. Fig. 2F) and the RLI was 4.6 ( $p < 0.001$ , Suppl. Table 1) indicating highly specific labelling. Taken together, these results indicate that both CD63 and the N-terminus of Nogo-A could be identified on the surface of EVs. The size range of Nogo-A+ EVs was comparable to the size range of CD63+ EVs, 80-100 nm (Suppl. Fig. 2F), consistent with the possibility of MVB-related biogenesis. The smaller proportion of Nogo-A+ vs CD63+ EVs is in line with the existence of different EV subpopulation.

Having found that the N-terminus of Nogo-A was on the extracellular face of the EV membrane on at least some of the Nogo-A+ EVs, we asked whether this is always the case, and whether the C-terminus is also on the outer surface. To this end, we generated flash-flag double tagged constructs of Nogo-A with the tag placed either near the C-terminus (Figure 3(a)) or on the hydrophilic N-terminus, after the functionally important Nogo-A- $\Delta$ 20 region (Figure 3(b)). Having validated the expression and proper trafficking of the constructs (Suppl. Fig. 3), we performed TEM imaging with immunogold labelling for the flag tag on EVs of HEK cells over-expressing the tagged Nogo-A.

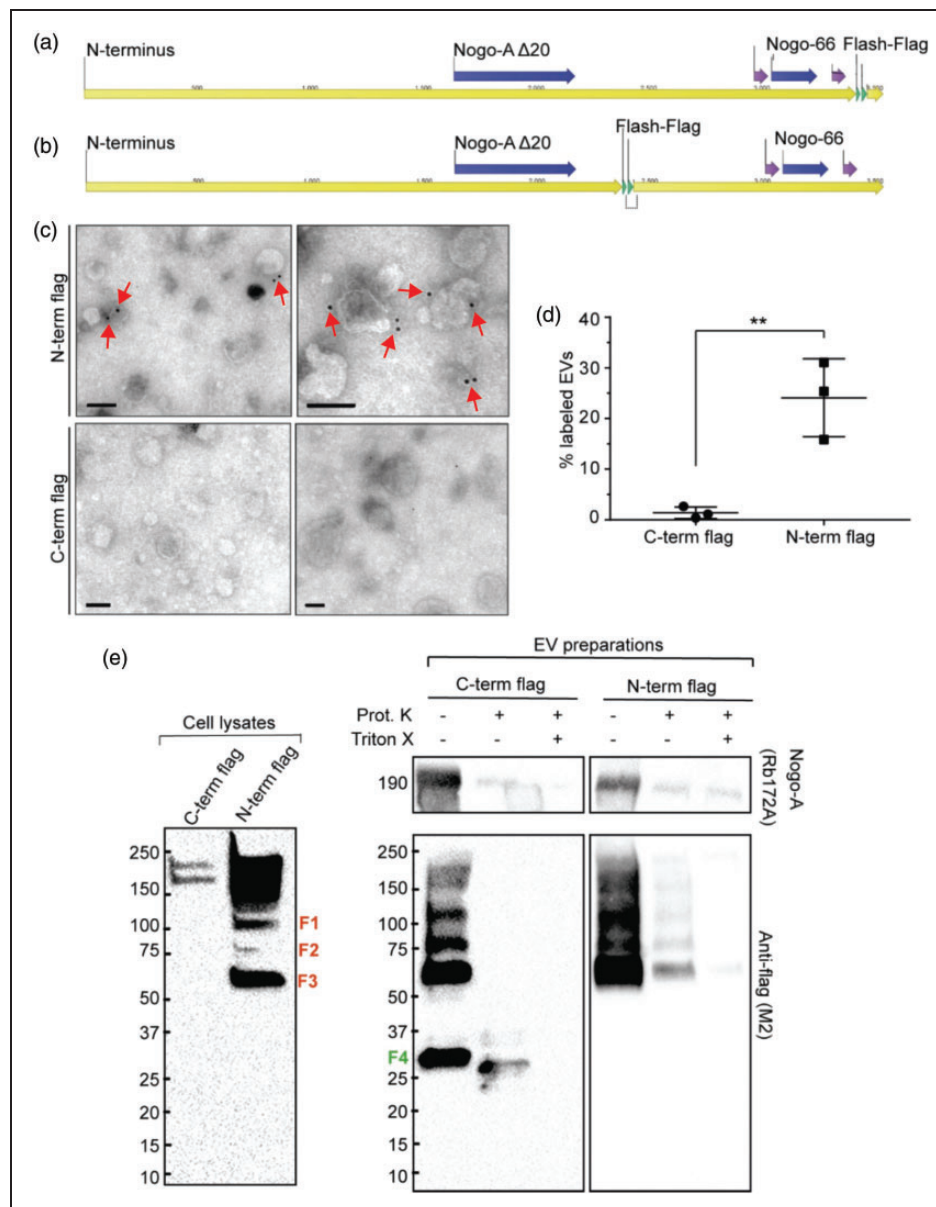


**Figure 3.** The C-terminus of Nogo-A is on the luminal side of extracellular vesicles (EVs), and the proteolytically sensitive N-terminus faces the extracellular space. (a) Map of the C-terminally flash-flag tagged construct of Nogo-A with the tag insertion site indicated in green arrow heads. (b) Map of the N-terminally flash-flag tagged Nogo-A construct. (c) Transmission electron microscopy (TEM) micrographs of EVs collected from HEK cells transfected with N-terminally (top) or C-terminally (bottom) tagged Nogo-A constructs. Scale bars = 100 nm. Red Arrows indicate positive labeling. (d) Quantification of the percentage of labeled EVs for N- and C-terminally tagged Nogo-A constructs. The statistical test performed was an unpaired student's t-test,  $p = 0.0072$ .  $n = 3$  independent EV isolations and (e) Western blots of from cells and EVs over-expressing either the N- or the C-terminally flag-tagged construct. Red labels F1–F4 indicate cleaved fragments of Nogo-A present in cell lysates and EVs. Green label F4 indicates a C-terminal cleaved fragment only found in EVs. For the limited proteolysis of EV samples, the EVs were treated with Proteinase K with or without permeabilization in 0.05% Triton X-100.

We found that  $24 \pm 7.7\%$  (mean  $\pm$  SD) of EVs were labelled when the tag was placed at the N-terminus, while  $1.4 \pm 1.2\%$  (mean  $\pm$  SD) were labelled when the tag was placed at the C-terminus (Figure 3(c) and (d)). The difference in labelling was significant ( $p = 0.0072$ ), indicating that the N-terminus, but not

the C-terminus, was accessible for EV surface labelling. This finding suggested an N-terminus outside/C-terminus inside topology for EV-associated Nogo-A.

We sought to confirm the suggested topology of EV-associated Nogo-A through treatment of permeabilized and non-permeabilized tagged EVs with proteinase K.

Through western blotting, we found that the band corresponding to full-length Nogo-A disappeared completely or almost completely upon proteinase K treatment of non-permeabilized EVs, indicating that all of the N-terminus was on the extracellular face (Figure 3(e)). Interestingly, we noted the presence of cleaved fragments at 120 kDa, 75 kDa and 60 kDa in untreated control EV samples (Figure 3(e)). A cleaved fragment of 30 kDa, corresponding to the molecular weight of the C-terminus and the transmembrane domain, was only present in C-terminally tagged samples. This finding indicated that the EV-bound Nogo-A was proteolytically processed at the N-terminus, and that a portion of the EV-bound Nogo-A consisted of only the transmembrane domain and the short C-terminus. The C-terminus was partially protected from proteinase K treatment in non-permeabilized samples (fragments in W-blot, Figure 3(e)) but was completely absent in permeabilized samples treated with proteinase K (Figure 3(e)). Taken together with the results from the TEM imaging, we conclude that the C-terminus is primarily on the luminal side of the EV membrane, but it is unclear if an alternate topology may exist to place the C-terminus on the extracellular face of the EV.

While we were able to confirm that all of the N-terminus of Nogo-A was on the extracellular face of the EV, the observed proteolytic processing suggested that the percentage of Nogo-A<sup>+</sup> EVs in the total population was probably underestimated. Interestingly, we also observed cleaved fragments down to the 60 kDa fragment in whole lysates of HEK cells overexpressing the tagged N-terminal construct, suggesting that some of the proteolytic processing occurs already within the cell (Figure 3(e)). The C-terminal 30 kDa fragment was exclusively found on the EVs, suggesting that the final cleavage occurs in an EV-associated manner (Figure 3(e)). These findings have been repeatedly validated with a similar outcome (Suppl. Fig 4). These results lead us to suggest that Nogo-A may be proteolytically processed along the biogenetic pathway of EV release, with final processing occurring on the EV surface.

### *EV-associated Nogo-A is active as a ligand*

We hypothesized that at least the portion of EVs with the N-terminus of Nogo-A intact could act as functional ligands to inhibit cell spreading and neurite outgrowth in a cell-to-cell contact-independent manner. Since we were specifically interested in the activity of the Nogo-A- $\Delta$ 20 region, we used a fibroblast spreading assay, which excludes any effect of Nogo-66.<sup>24</sup> In initial experiments we used spinal cord extract (SCE), known for its high levels of Nogo-A,<sup>39</sup> as a positive control. We found that wild type (WT) N2a neuroblastoma cell

derived EVs were highly inhibitory for fibroblast spreading when applied in solution at either 20  $\mu$ g/ml or 100  $\mu$ g/ml (Figure 4(a) and (b)). Strikingly, 20  $\mu$ g/ml EVs was as inhibitory as 80  $\mu$ g/ml SCE, and there was no further increase in spreading inhibition when EVs were applied at the higher concentration of 100  $\mu$ g/ml (Figure 4(b)). EV-depleted supernatants of ultracentrifugation carried only extremely low inhibitory activity at very high concentrations when either coated or in solution (Figure 4(c) and (d)), suggesting that the inhibitory activity is not associated with possible soluble fragments of Nogo-A. Importantly, eGFP containing EVs did not show any inhibitory effects (Suppl. Fig. 5). Taken together, these results suggested that EV-associated Nogo-A may be active as a signaling ligand, and that the inhibitory activity was specifically associated with the EV fraction.

We then tested a range of EV concentrations in the fibroblast spreading assay to find the IC<sub>50</sub>, i.e. the concentration at which the spreading was reduced by 50% over the range of possible values from unspread to fully spread cells. Through non-linear regression analysis, we found that the IC<sub>50</sub> shifted depending on the EV preparation (Figure 4(d)). The lowest IC<sub>50</sub> range was 2.7–7.7  $\mu$ g/ml, and the highest IC<sub>50</sub> range was 13.6–21.1  $\mu$ g/ml. Since both the Hill slope and the IC<sub>50</sub> were significantly different for each EV preparation ( $p < 0.0001$ ), the fitting of an average curve to model all the data was not appropriate. To compare these values directly to the SCE, we applied the SCE in solution onto fibroblasts, and found that the IC<sub>50</sub> of one SCE preparation was in the range of 16.09–23.2  $\mu$ g/ml (Figure 4(e)).

### *Nogo-A<sup>+</sup> EVs signal via S1PR2*

To unravel the signaling pathways underlying the observed spreading inhibition upon treatment with Nogo-A<sup>+</sup> EVs, we asked whether the Nogo-A- $\Delta$ 20 receptor S1PR2 might be involved. To this end, we pre-treated fibroblasts with the S1PR2 antagonist JTE-013 or vehicle dimethyl sulfoxide (DMSO) and assessed the spreading inhibition in the presence of Nogo-A<sup>+</sup> EVs from either WT N2a or WT Oli-neu cells, applied at the estimated IC<sub>50</sub>. Similar to the results described above, we observed spreading inhibition upon treatment with N2a and Oli-neu EVs in the presence of vehicle (DMSO) (Figure 5(a) and (b)). With the IC<sub>50</sub> concentration of EVs resulting in 60–70% spreading inhibition for N2a EVs and Oli-neu EVs we observed a partial recovery of spreading inhibition of both N2a and Oli-neu EVs upon treatment with JTE-013 (Figure 5(b) and (c)). When analysed as percent change in cell surface area with JTE over DMSO, the recovery was statistically significant ( $p = 0.0301$ )



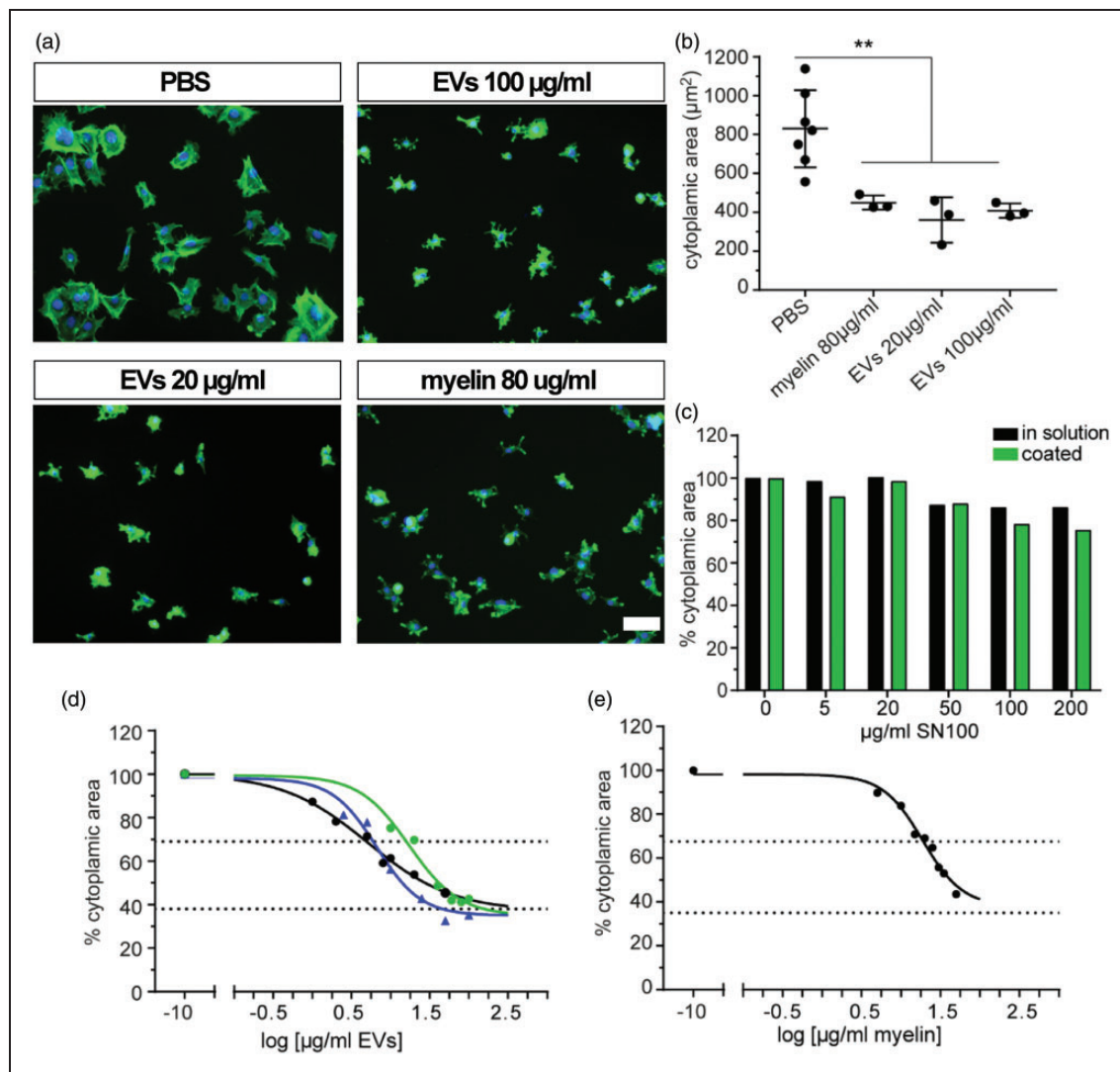


**Figure 4.** EV-associated Nogo-A is active as an inhibitor of fibroblast spreading. Fibroblasts were plated in the presence of N2a EVs or proteins from the supernatant of ultracentrifugation (SN100) for 1 h at 37 °C, and cell spreading was quantified thereafter as cytoplasmic area. PBS or spinal cord extract ('myelin') were used as negative and positive controls respectively. (a) Images of fibroblasts treated PBS, myelin or N2a cell-derived EVs. Green=phalloidin (cytoskeleton), Blue=DAPI (nuclei). (b) Quantification of cell spreading in the presence of myelin or N2a EVs from  $n = 3$  independent experiments. (c) Quantification of cell spreading in the presence of SN100, either coated or in solution as indicated. (d) Dose-response curve of fibroblast spreading in the presence of N2a-derived EVs. Each curve represents one independent EV isolation, 3 replicate wells at each concentration and (e) the values determined from one myelin preparation, 3 replicate wells at each concentration. Scale bar = 20 µm.

for N2a EVs (Figure 5(c)). We therefore conclude that the spreading inhibition is at least partially mediated by S1PR2.

#### *Nogo-A associated EVs are present in physiological blood samples*

As shown above, Nogo-A<sup>+</sup> vesicles are secreted into culture supernatants of several cell lines, including CNS-derived cells. We then investigated whether Nogo-A<sup>+</sup> EVs can be found in body fluids *in vivo*, in particular blood. Blood serum and plasma were

collected from healthy, adult C57Bl6 mice, Long-Evans rats, and human blood donors. To be able to detect also very low levels of Nogo-A<sup>+</sup> EVs, a highly sensitive capture ELISA was developed: a monoclonal mouse anti-Nogo-A antibody was used to capture Nogo-A on the ELISA plate, and a polyclonal anti-Nogo antibody was added for detection. The limit of detection (LOD) and limit of quantification (LOQ) for Nogo-A was determined using a standard curve of recombinant Nogo-A  $\Delta 20$  fragment. We were able to reach a total Nogo-A sensitivity of 147 pM (limit of detection (LOD), OD<sub>450</sub> = 0.005), or respectively

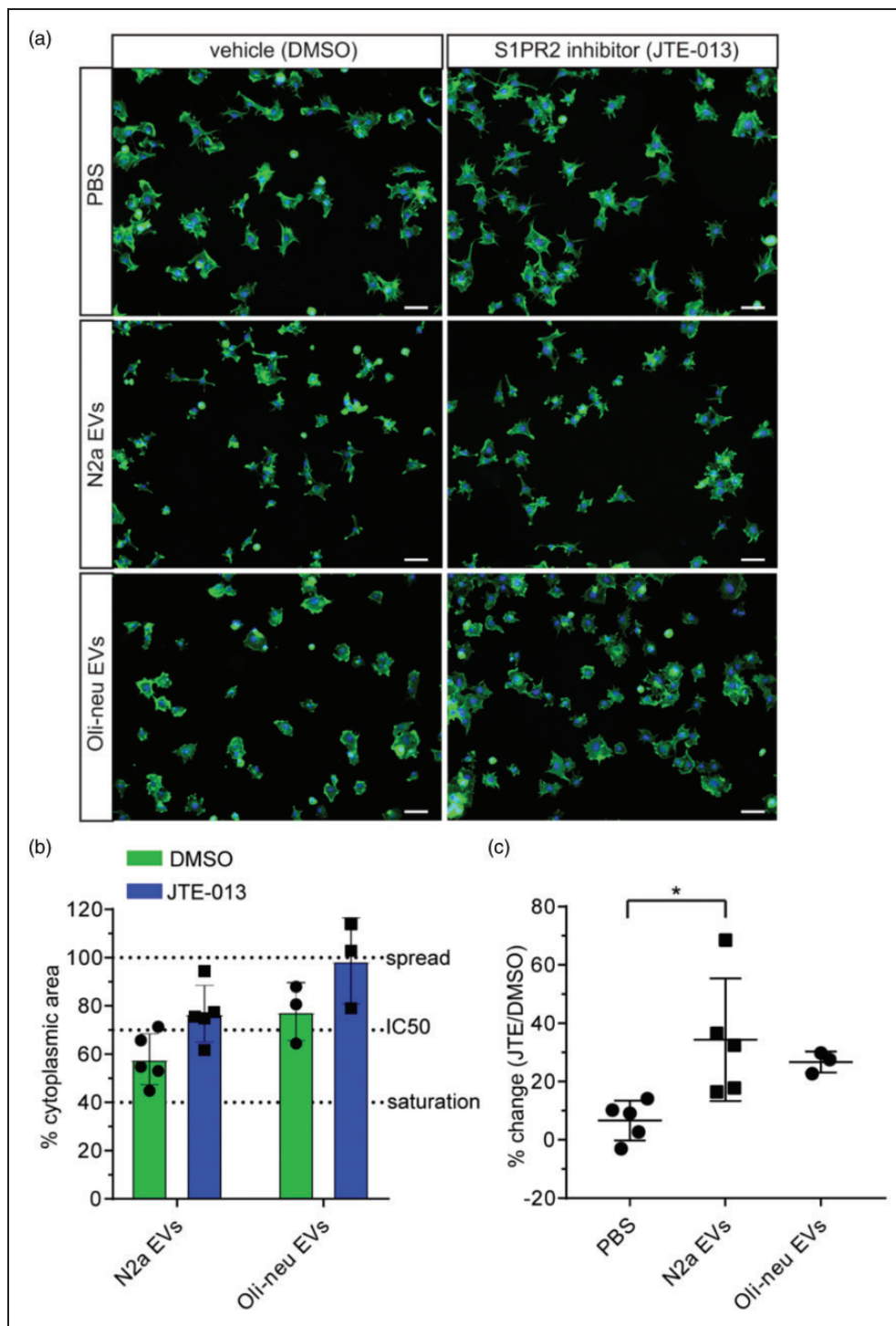


**Figure 5.** Nogo-A+ EV-induced spreading inhibition is partially recovered by S1PR2 blockade. Fibroblasts were pre-treated with 10  $\mu$ M JTE-013 or vehicle (DMSO) and plated at 37  $^{\circ}$ C for 1 h in the presence of EVs or control (PBS). (a) Images of fibroblast spreading with vehicle or JTE-013 treatment. Green=phalloidin (cytoskeleton), blue = DAPI (nuclei). (b) Quantification of the inhibition achieved with EVs, and the recovery with JTE-013 treatment, normalized to the control (PBS) condition and (c) Analysis of the percent change in cytoplasmic area upon JTE treatment relative to the DMSO control. The statistical test performed was a one-way ANOVA with a Bonferroni multiple comparisons test. Scale bar = 20  $\mu$ m.

490 pM (limit of quantification (LOQ), OD450 = 0.083, Figure 6(a)). The analysis of the blood-derived samples revealed the presence of Nogo-A in the blood of all mice, rats, and humans. The Nogo-A concentrations in the serum of healthy mice and rats were comparable (mouse = 0.76 nM, rat = 0.52 nM), whereas we observed 10–15 fold increased Nogo-A concentrations in human plasma samples (human = 8.65 nM, Figure 6(b)). To assess if the serum Nogo-A was associated with EVs, we modified the ELISA by capturing Nogo-A with an anti-Nogo-A antibody and detecting the EVs with anti-CD63 antibodies. We detected CD63-associated Nogo-A in mouse and human blood samples (mice = 0.25 nM, human = 0.95 nM) although at seemingly lower concentrations than Nogo-A alone (Figure 6(c)), a result which might also be influenced by the unknown relative antibody affinities used in the ELISA.

These results show that Nogo-A+ EVs are present *in vivo* and secreted into blood, implying the potential to act at a long range.

Blood levels of Nogo-A peptides are elevated in rodent models of ischemic stroke

Since high levels of Nogo-A and one of its receptors S1PR2 are present in the adult brain and are known to be elevated following cerebral ischemia,<sup>3,40</sup> we hypothesized that Nogo-A may be released into the blood circulation following brain injury at higher concentrations.

We induced a large photothrombotic stroke ( $3.1 \pm 1.2 \text{ mm}^3$ ) in the right sensorimotor cortex of C57Bl6 mice and collected blood from the tail vein at preoperative baseline, and 7 and 15 days after stroke (Figure 6 (d), (e) and (g)). Histological sections of stroked brains showed a typical local inflammatory response (Iba1<sup>+</sup>), glial scar formation (GFAP<sup>+</sup>) and vascular disruption (CD31) in the ipsilesional hemisphere, which were absent in the intact, contralesional site (Figure 6(f)). A significant increase of Nogo-A immunoreactivity in the serum was observed after cerebral ischemia at 7 dpi (+51%;  $1.17 \pm 0.42 \text{ nM}$ ) and 14 dpi (+54%,  $1.18 \pm 0.37 \text{ nM}$ ) compared to healthy mice ( $0.76 \pm 0.07 \text{ nM}$ ) (Figure 6(g)). The continuous presence of Nogo-A in the blood serum was independently confirmed in an equivalent rat model of stroke (Suppl. Fig. 6).

### Secreted Nogo-A is associated with increased vascular permeability

Since the sphingosine 1-phosphate receptor S1PR2, which can also act as a Nogo-A receptor and signal transducer,<sup>9</sup> is highly expressed on the vascular endothelium and has been previously shown to regulate permeability and inflammation of the vasculature,<sup>41,42</sup> we hypothesized that long-range Nogo-A signaling may

influence vascular functions in the CNS and beyond. To test this hypothesis, we first used an *in vitro* blood-brain barrier model consisting of primary mouse brain vascular endothelial cells co-cultured with primary astrocytes in a cell culture insert.<sup>43</sup> These assays, and even more so the *in vivo* studies shown below, required amounts of active Nogo-A far beyond of what could be obtained in the form of purified Nogo-A+ EVs from cell cultures. For this reason and also for the sake of specificity, we used the well characterized active Nogo-A peptide Nogo-A  $\Delta 20$ .<sup>9</sup> Nogo-A  $\Delta 20$  was added at 1  $\mu\text{M}$  and 10  $\mu\text{M}$  concentrations from the luminal (vascular endothelium) or abluminal (astrocyte) side and compared to VEGF, a potent enhancer of vascular permeability. Concentrations were chosen according to previous *in vitro* assays.<sup>9,24</sup>

Nogo-A peptide acting from the luminal surface of cultured brain endothelial cells induced a 10–20% concentration dependent decrease in the impedance of the monolayer, an indicator of barrier tightness drop (Figure 7(b)). Interestingly, although Nogo-A and VEGF decreased the impedance to a similar extent, the effect of Nogo-A occurred earlier (4–16 h) than that of VEGF (14–25 h). No changes in the trans-endothelial electrical resistance (TEER) of cultured brain endothelial cells in the BBB co-culture model could be detected 6 h following treatment with Nogo-A  $\Delta 20$  peptide (Figure 7(c), control  $65.13 \pm 6.05 \text{ Ohm} \times \text{cm}^2$ ; Nogo-A abluminal treatment:  $63.60 \pm 12.22 \text{ Ohm} \times \text{cm}^2$ ; Nogo-A luminal treatment:  $60.25 \pm 6.64 \text{ Ohm} \times \text{cm}^2$ ; VEGF treatment:  $15.68 \pm 4.50 \text{ Ohm} \times \text{cm}^2$ ). Importantly, the observed tightness in the control group was above the critical threshold for an *in vitro* barrier model showing proper tight junction integrity and low permeability.<sup>44</sup> We further investigated the barrier integrity changes on the BBB co-culture model using two fluorescent markers, sodium fluorescein (SF) and Evans blue labeled albumin (EBA). We found increased permeability of cultured brain endothelial cells for both fluorescent markers (SF: +76%; EBA: +105%) following the administration of Nogo-A  $\Delta 20$  compared to the control, in agreement with the impedance data (Figure 7(d)). However, the effect was lower than that of VEGF (SF: +190%, EBA +440%) and concentration dependent, since we did not observe a change in dye permeability following Nogo-A  $\Delta 20$  administration at the lower 1  $\mu\text{M}$  concentration (Figure 7(d)).

Next, we asked if Nogo-A or its active fragment Nogo-A  $\Delta 20$  may also increase the permeability in the peripheral vasculature. Therefore, stroked and control mice were systemically injected with Evans's blue (EB) to label circulating albumin 30 min. before perfusion and sacrifice. Peripheral organs were removed including (heart, kidney, liver, lung, muscle, and skin) and leaked EB signal was measured. We identified

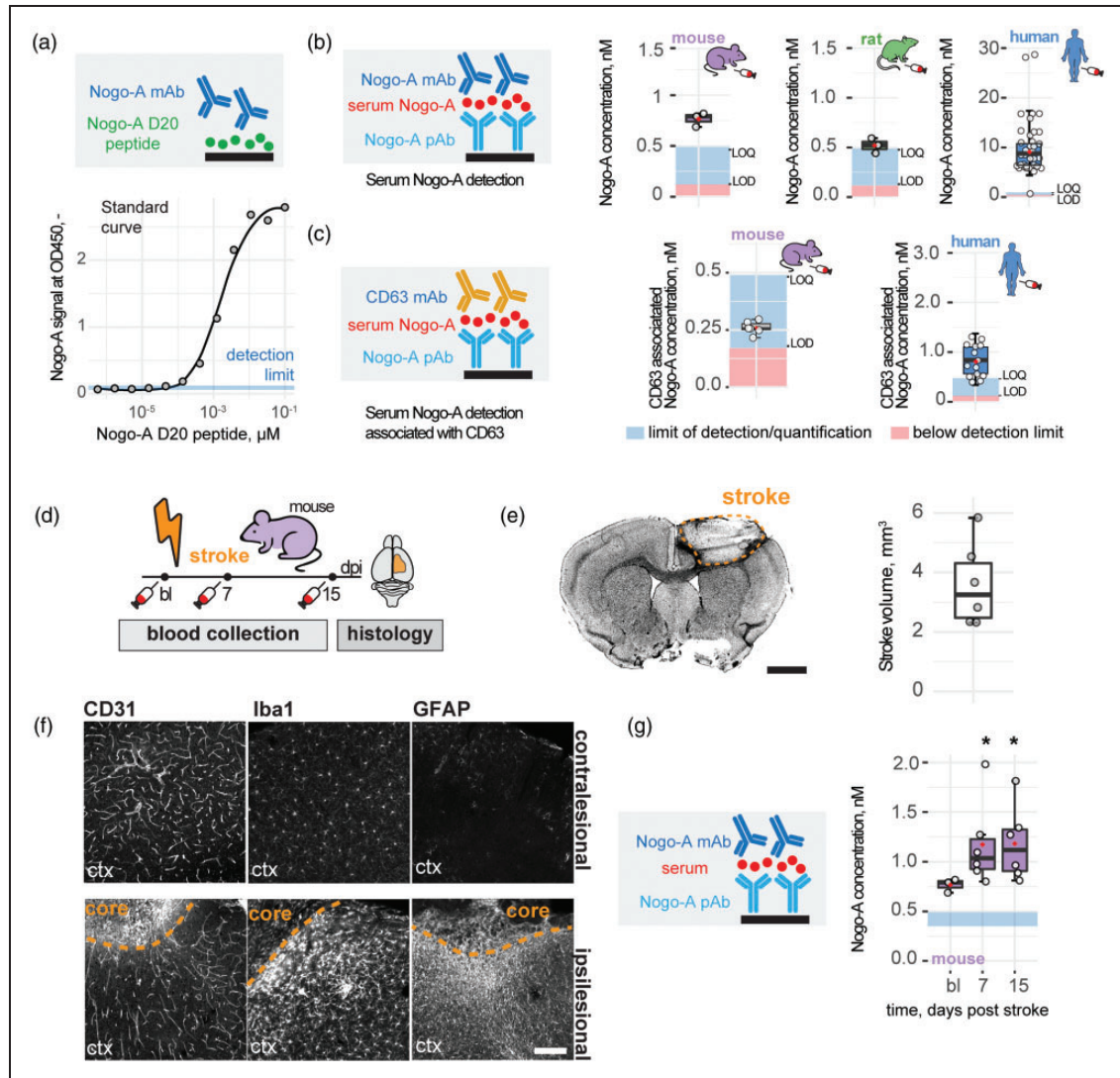


**Figure 6.** Nogo-A in serum of adult mouse, rat, human and in mice after focal cerebral stroke. (a) Assay development: Binding of Nogo-A antibody to Nogo-A  $\Delta$ 20, limit of detection and quantification. (b) Capture ELISA for Nogo-A; results for blood-derived samples of mice, rats, and humans. (c) Detection of CD63-associated with Nogo-A<sup>+</sup> EVs by capture ELISA, results for blood serum in mice and plasma in humans. (d) Scheme of experimental design of stroke study in mice. (e) Representative micrograph of stroked brain visualized with Nissl staining, scale bar: 500  $\mu$ m. Quantitative measure of stroke volume in mm<sup>3</sup>. (f) Representative immunofluorescence images of contralateral, intact (upper row) and ipsilesional, stroked (lower row) cortex with astrocytes (GFAP), microglia (Iba1) and vasculature (CD31) at 15 days post injury (dpi). Scale bar 100  $\mu$ m and (g) Quantitative assessment of Nogo-A in mouse serum at baseline (intact), at 7 dpi and 15 dpi. The statistical test performed was a one-way ANOVA with a Bonferroni multiple comparisons.

increased EB signals in the heart (+21%), kidney (+19%), liver (109%) and skin (+128%) of stroked mice compared to the intact controls (Figure 7(e)). To assess if the increased permeability effects could be due to Nogo-A, we used the Miles assay, an *in vivo* method to assess permeability of the skin vasculature. EB dye was systemically injected followed by multiple intradermal injections of Nogo-A  $\Delta$ 20, VEGF, or a vehicle control into opposing flanks of the same mouse. Thirty min. after EB injection, we detected

increased permeability in skin treated with Nogo-A peptide (+32%) or VEGF (+66%) compared to the control injections (Figure 7(f)).

## Discussion

In the present study we show that full-length Nogo-A can be secreted on the surface of exosome-like EVs of approximately 100 nm in diameter by cultured neurons and oligodendrocytes, i.e. by the *in vivo*-Nogo-A

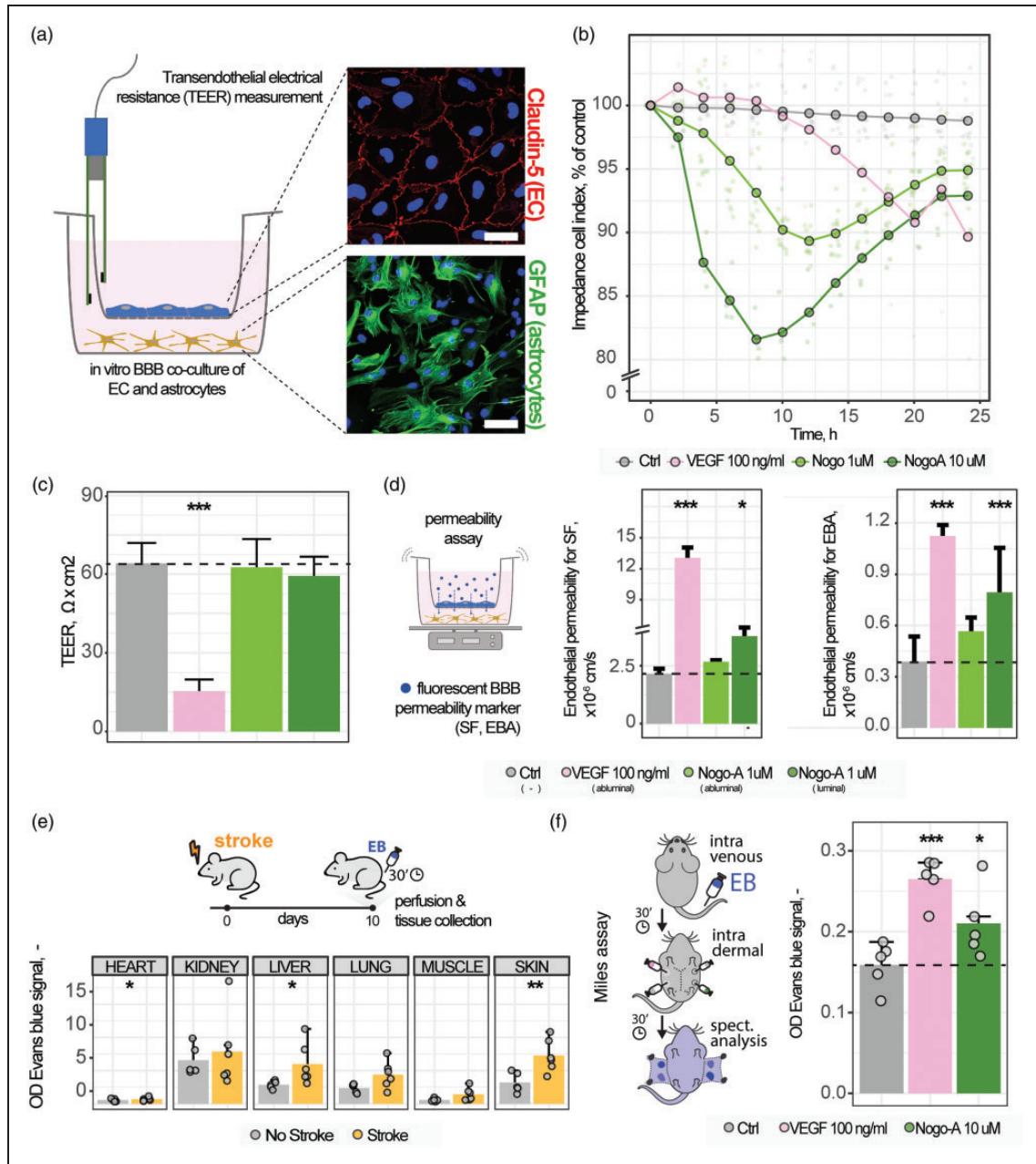


**Figure 7.** Nogo-A regulates vascular permeability in CNS and non-CNS vasculature. (a) Schematic representation of the *in vitro* BBB model. (b) Real-time impedance measurement at 10'000 Hz after luminal administration of cell culture medium (Ctrl), VEGF (100 ng/ml) or Nogo-A  $\Delta$ 20 (1  $\mu$ M, 10  $\mu$ M) measuring ion flow between cells. (c) Transendothelial electrical resistance measurement (TEER) at 12.5 Hz after luminal (endothelial side) and abluminal (astrocyte side) administration of cell culture medium (Ctrl), VEGF (100 ng/ml) or Nogo-A  $\Delta$ 20 (1  $\mu$ M, 10  $\mu$ M) measuring paracellular ion permeability after 6 h. (d) Permeability measurement for fluorescent marker molecules sodium fluorescein (SF) and Evans blue labeled albumin (EBA) after luminal and abluminal VEGF or Nogo-A  $\Delta$ 20 treatment. (e) Vascular permeability for systemic Evans Blue (EB) in intact vs. stroke mice. Quantitative assessment of EB signal in peripheral organs incl. heart, kidney, liver, lung, muscle, and skin and (f) Intradermal injection of VEGF or Nogo-A  $\Delta$ 20 induces local permeability changes (Miles assay). The statistical test performed were t-tests to compare two groups (in e), and a one-way ANOVA with Bonferroni multiple comparisons test to compare multiple groups (in c,d,f).

producing cell types. The N-terminus of Nogo-A was found to be facing the extracellular space, and it was active as a ligand inhibiting fibroblast spreading. Partial recovery of Nogo-A+ EV-mediated spreading

inhibition was achieved through S1PR2 blockade, indicating that EV-associated Nogo-A signals, at least in part, through this receptor. The possibility of *in vivo* relevance of Nogo-A positive EVs was raised by our

detection of EVs in blood of healthy rodents and humans. Interestingly, blood Nogo-A levels were elevated after cerebral stroke in rodents; an increased vascular permeability across different peripheral organs was also observed in these stroked mice. Exposure of *in vitro* BBB tissue to active Nogo-A peptide increased BBB permeability. *In vivo*, skin vessel permeability was also increased by Nogo-A. The present results show the occurrence of soluble, EV-bound Nogo-A in body fluids and point to a possible role of soluble Nogo-A in the regulation of vascular permeability.

In the oligodendrocytes and neurons, Nogo-A is found in low but functionally relevant amounts at the plasma and myelin membrane, and in a higher abundance at the ER membrane.<sup>24,25,38</sup> At the cell surface, the N-terminus of Nogo-A faces the extracellular space.<sup>24,25,45</sup> Herein, we found that the N-terminus of Nogo-A was present on the outer surface of the EVs. This finding is consistent with a plasma membrane or multivesicular body/endosome-related biogenesis of the Nogo-A<sup>+</sup> EVs. Density gradient fractionation suggested that Nogo-A is present in a Flotillin-1+ subpopulation of EVs. The Flotillins are lipid raft-associated scaffolding proteins,<sup>46</sup> which have previously been shown to be associated with ESCRT-independent and ceramide-dependent trafficking of proteolipid protein (PLP) into exosomes in oligodendrocytes.<sup>47</sup> The slightly higher buoyancy of Flotillin-1+ EVs compared to EVs containing ESCRT components has also been noted by others.<sup>48</sup> Taken together with our findings of low levels of the ESCRT-associated protein Alix in EVs from Nogo-A over-expressing HEK cells, we suggest that Nogo-A may be sorted into EVs in an ESCRT-independent and perhaps lipid raft-dependent manner. Whether the Flotillin+ and Nogo-A+ EVs represent a distinct functional subpopulation of EVs remains to be further investigated. This possibility is supported by the finding of a discrete buoyancy of this population in the density gradient as discussed above. It has recently been shown that N2a cells secrete discrete subpopulations of EVs, which have different effects on the gene expression of target cells.<sup>49</sup> Interestingly, EphA2 appeared to be enriched in the high density (low buoyancy) subpopulation in this study. Moreover, the developmentally important lipid-modified morphogen sonic hedgehog (SHH) was recently described to be sorted into two different populations of EVs with distinct signaling properties.<sup>50</sup> Intriguingly, only SHH+ EVs which contained also integrins and were part of the Flotillin+ subpopulation could activate endogenous target genes of SHH. These findings support the concept that distinct subpopulations of EVs may play defined roles in signaling. Whether this is the case for Nogo-A EVs as well remains to be determined. As Flotillin-1 was recently

found in multiple subpopulations of EVs,<sup>51</sup> it does not serve as a unique marker of a distinct subpopulation, and therefore further investigation is required to define the possible Nogo-A enriched subpopulation(s).

We also found that Nogo-A was proteolytically processed at multiple sites. The most prominent cleaved fragments were a 60 kDa fragment, which was present in both cell lysates and EVs, and a 30 kDa fragment, which was only present in EVs. Sekine *et al.* also found an EV-associated 24 kD C-terminal Nogo-A fragment produced by BACE-1 activity in culture supernatant of Nogo-A transfected HEK cells and at increased levels in extracts of spinal cord injured CNS tissue.<sup>14</sup> This fragment contains the active Nogo-66 sequence and inhibits neurite outgrowth *in vitro* and *in vivo*.<sup>14</sup> Unlike the findings by Sekine *et al.*, our data suggests that the majority of EV-associated Nogo-A contains full length Nogo-A with a N-terminus outside/C-terminus inside topology. We showed that the EV-associated N-terminus of Nogo-A was active in inhibiting fibroblast spreading, much more than the cleavage products in the supernatant. This finding supports the concept that the N-terminus of Nogo-A is most active on the surface of membranes, perhaps in oligomerized form as noted by others.<sup>24,52</sup> This follows along the same lines as has been shown for ephrins, which cluster at membranes and are proteolytically processed in multiple ways, but are weak agonists of their respective binding partners in the soluble, unclustered form.<sup>53-56</sup> However, orientation and proteolytic process of Nogo-A for long-range signaling may be context-dependent and vary across cell types and experimental conditions.<sup>14</sup>

As expected, the EV-bound Nogo-A appeared to signal, at least in part, through the Nogo-A receptor S1PR2, as has been shown for purified substrate-bound Nogo-A  $\Delta$ 20 fragment.<sup>9</sup> For the purified Nogo-A  $\Delta$ 20, the recovery of spreading inhibition by S1PR2 blockade was also partial, and full recovery could only be achieved with concomitant blockade of HSPGs.<sup>9,11</sup>

Based on the topology of EV-bound Nogo-A described herein, we would expect the Nogo-66 region to be on the extracellular face of the EV membrane as well. Indeed, EVs containing an active, C-terminal 24 kD Nogo-A fragments including the Nogo-66 sequence have been shown to inhibit neurite outgrowth *in vitro* and *in vivo*.<sup>14</sup> Growth cone collapse of dorsal root ganglion (DRGs) neurites was recently observed in response to EphB2+ EVs,<sup>56</sup> and increased neurite outgrowth on CNS inhibitory substrates upon treatment with fibroblast-derived EVs was recently reported.<sup>57</sup> Therefore, EV-bound ligands have the capability to affect neurite outgrowth. However, a complication of these assays is that it is extremely difficult to observe the neuronal response to a single factor, since

EV preparations contain multiple factors, including miRNAs, which can influence gene expression through multiple pathways within the long incubation times required for outgrowth assays.

The presence of Nogo-A<sup>+</sup> EVs in blood could suggest that they play a signaling role *in vivo* in the vessel system, e.g., via the vascular endothelium associated receptor S1PR2. Previous work showed a role of Nogo-A/S1PR2 in CNS vascular development, maturation, and remodeling after injury.<sup>3,4,29</sup> Endothelial S1PR2 has also been described as a key regulator of vascular permeability and inflammation.<sup>41</sup> Indeed, the present results show that mice with large cortical strokes showed increased vascular permeability in various organs 2 weeks after the stroke when compared to intact, naïve mice as determined by Evans blue tissue concentrations 30 min. after i.v. injection. The underlying mechanism is not entirely clear. There is evidence that a systemic release of pro-inflammatory mediators including cytokines (such as IL-1 $\beta$ , IL-6, TNF- $\alpha$ , and IFN- $\gamma$ ) and chemokines (CXCL-1, CXCL2) occurs following experimental stroke.<sup>58–60</sup> These pro-inflammatory mediators can affect peripheral vascular endothelium and influence its permeability.<sup>61,62</sup> For instance, damage to the intestine-blood barrier<sup>63</sup> has been described following experimental stroke, as well as changes in the lung vascular permeability.<sup>64</sup> To our knowledge there is no systematic study looking at peripheral vascular permeability after cerebral stroke.

Cultured primary mouse brain endothelial cells responded to the active, S1PR2 binding Nogo-A fragment D20 with decreased electrical resistance and increased dye permeability, similar to the known permeability enhancer VEGF.<sup>65</sup> Skin permeability in mice was also enhanced by Nogo-A  $\Delta$ 20. These results suggest that blood borne Nogo-A including Nogo-A-containing EVs might exert a regulatory effect on central and peripheral blood vessels. Our *in vitro* data suggests that Nogo-A EVs may signal via the receptor S1PR2, which is expressed on the peripheral vascular endothelium and an important regulator of vascular permeability.<sup>41</sup> Future studies could extend these findings by exploring changes in peripheral vascular permeability after stroke in Nogo-A and S1PR2 deficient mice.

The source of the blood-borne Nogo-A<sup>+</sup> EVs is currently unknown. Although Nogo-A associated with EVs has been detected in healthy humans as well as mice and rats, the exact ratio of Nogo-A present in EVs over total Nogo-A or Nogo fragments in rodent stroke models has not been determined due to limited sample volume. However, it is conceivable that blood borne Nogo-A exist in several forms including EVs as well as fragments.

A CNS origin of blood Nogo-A EVs in mice after large cortical strokes as shown here seems plausible.

Neutralization of Nogo-A by antibodies after cortical strokes in mice was shown to enhance vascular repair in the stroke penumbra.<sup>3,29,31</sup> In stroked rats, intrathecal Nogo-A antibodies enhanced neuritic sprouting, circuit plasticity and functional recovery.<sup>66,67</sup> Roles of Nogo-A or its inactivation in the periphery of the body have not been investigated so far. The potential function of Nogo-A<sup>+</sup> EVs in the intact vessel system and body therefore remains an intriguing unanswered question. Long-range effects of soluble, blood or tissue fluid carried Nogo-A have not been described so far. The present indications for a regulatory action on blood vessel permeability open new avenues to deepen mechanistic insights into the (patho-)physiological role of Nogo-A during health and disease.

### Funding

The author(s) received no financial support for the research, authorship, and/or publication of this article.

### Declaration of conflicting interests

The author(s) declared the following potential conflicts of interest with respect to the research, authorship, and/or publication of this article: M.E.S. is a founder and CEO of the University of Zurich spin-off company NovaGo Therapeutics Inc. seeking at developing antibody based therapies for neurological diseases. M.A.M. is under paid employment of NovaGo Therapeutics. Otherwise, the authors have no patents pending or financial conflicts to disclose.

### Authors' contributions


R.R., M.M.H, M.E.S., F.W., I.H. designed the study. R.R., M.M.H, F.W., A.R.S.M., M.D., M.E.S prepared the figures and wrote the manuscript. R.R., M.M.H, M.E., O.W., D.v. R., F.W., A.R.S.M., L.G., M.A.M., R.C., S.K., A.A., carried out experiments, A.A., T.F.L. provided human samples. All authors read and approved the final manuscript.


### Supplementary material

Supplemental material for this article is available online.

### ORCID iDs

Ruslan Rust  <https://orcid.org/0000-0003-3376-3453>

Michael A Maurer  <https://orcid.org/0000-0003-1504-7285>

Alexander Akhmedov  <https://orcid.org/0000-0003-3052-9493>

### References

- Schwab ME and Strittmatter SM. Nogo limits neural plasticity and recovery from injury. *Curr Opin Neurobiol* 2014; 27: 53–60.
- Kempf A and Schwab ME. Nogo-A represses anatomical and synaptic plasticity in the Central nervous system. *Physiology (Bethesda)* 2013; 28: 151–163.

3. Rust R, Grönnert L, Gantner C, et al. Nogo-A targeted therapy promotes vascular repair and functional recovery following stroke. *Proc Natl Acad Sci USA* 2019; 116: 14270–14279.
4. Wälchli T, Pernet V, Weinmann O, et al. Nogo-A is a negative regulator of CNS angiogenesis. *Proc Natl Acad Sci USA* 2013; 110: E1943–1952.
5. Wang X, Chun S-J, Treloar H, et al. Localization of Nogo-A and nogo-66 receptor proteins at sites of axon-myelin and synaptic contact. *J Neurosci* 2002; 22: 5505–5515.
6. Petrinovic MM, Hourez R, Aloy EM, et al. Neuronal Nogo-A negatively regulates dendritic morphology and synaptic transmission in the cerebellum. *Proc Natl Acad Sci USA* 2013; 110: 1083–1088.
7. Zemmar A, Weinmann O, Kellner Y, et al. Neutralization of Nogo-A enhances synaptic plasticity in the rodent motor cortex and improves motor learning in vivo. *J Neurosci* 2014; 34: 8685–8698.
8. Ahmed Z, Douglas MR, John G, et al. AMIGO3 is an NgR1/p75 Co-Receptor signalling axon growth inhibition in the acute phase of adult central nervous system injury. *PLoS ONE* 2013; 8: e61878.
9. Kempf A, Tews B, Arzt ME, et al. The sphingolipid receptor SIPR2 is a receptor for nogo-a repressing synaptic plasticity. *PLoS Biol* 2014; 12: e1001763.
10. Thiede-Stan NK, Tews B, Albrecht D, et al. Tetraspanin-3 is an organizer of the multi-subunit Nogo-A signaling complex. *J Cell Sci* 2015; 128: 3583–3596.
11. Kempf A, Boda E, Kwok JCF, et al. Control of cell shape, neurite outgrowth, and migration by a Nogo-A/HSPG interaction. *Developmental Cell* 2017; 43: 24–34.e5.
12. Fournier AE, Takizawa BT and Strittmatter SM. Rho kinase inhibition enhances axonal regeneration in the injured CNS. *J Neurosci* 2003; 23: 1416–1423.
13. Belien A T, Paganetti P. a and Schwab ME. Membrane-type 1 matrix metalloprotease (MT1-MMP) enables invasive migration of glioma cells in central nervous system white matter. *J Cell Biol* 1999; 144: 373–384.
14. Sekine Y, Lindborg JA and Strittmatter SM. A proteolytic C-terminal fragment of Nogo-A (reticulon-4A) is released in exosomes and potently inhibits axon regeneration. *J Biol Chem* 2020; 295: 2175–2183.
15. Colombo M, Raposo G and Théry C. Biogenesis, secretion, and intercellular interactions of exosomes and other extracellular vesicles. *Annu Rev Cell Dev Biol* 2014; 30: 255–289.
16. Fauré J, Lachenal G, Court M, et al. Exosomes are released by cultured cortical neurones. *Molecular and Cellular Neurosciences* 2006; 31: 642–648.
17. Frühbeis C, Fröhlich D, Kuo WP, et al. Neurotransmitter-Triggered transfer of exosomes mediates oligodendrocyte-neuron communication. *PLoS Biol* 2013; 11: e1001604.
18. Goldie BJ, Dun MD, Lin M, et al. Activity-associated miRNA are packaged in Map1b-enriched exosomes released from depolarized neurons. *Nucleic Acids Res* 2014; 42: 9195–9208.
19. Korkut C, Li Y, Koles K, et al. Regulation of postsynaptic retrograde signaling by presynaptic exosome release. *Neuron* 2013; 77: 1039–1046.
20. Fröhlich D, Kuo WP, Frühbeis C, et al. Multifaceted effects of oligodendroglial exosomes on neurons: impact on neuronal firing rate, signal transduction and gene regulation. *Phil Trans R Soc B* 2014; 369: 20130510–20130510.
21. Lopez-Verrilli MA, Picou F and Court FA. Schwann cell-derived exosomes enhance axonal regeneration in the peripheral nervous system. *Glia* 2013; 61: 1795–1806.
22. Korkut C, Ataman B, Ramachandran P, et al. Trans-synaptic transmission of vesicular wnt signals through evi/wntless. *Cell* 2009; 139: 393–404.
23. Gross JC, Chaudhary V, Bartscherer K, et al. Active wnt proteins are secreted on exosomes. *Nat Cell Biol* 2012; 14: 1036–1045.
24. Oertle T, van der Haar ME, Bandtlow CE, et al. Nogo-A inhibits neurite outgrowth and cell spreading with three discrete regions. *J Neurosci* 2003; 23: 5393–5406.
25. Dodd DA, Niederoest B, Bloechlinger S, et al. Nogo-A, -B, and -C are found on the cell surface and interact together in many different cell types. *J Biol Chem* 2005; 280: 12494–12502.
26. Gibson DG, Young L, Chuang R-Y, et al. Enzymatic assembly of DNA molecules up to several hundred kilobases. *Nat Methods* 2009; 6: 343–345.
27. Théry C, Clayton A, Amigorena S, et al. Isolation and characterization of exosomes from cell culture supernatants. *Curr Protoc Cell Biol* 2006; Chapter 3: Unit 3.22.
28. Van Deun J, Mestdagh P, Sormunen R, et al. The impact of disparate isolation methods for extracellular vesicles on downstream RNA profiling. *J Extracellular Vesicles* 2014; 3: 1–14.
29. Rust R, Weber RZ, Grönnert L, et al. Anti-Nogo-A antibodies prevent vascular leakage and act as pro-angiogenic factors following stroke. *Sci Rep* 2019; 9: 20040.
30. Rust R, Weber RZ, Generali M, et al. Xenon-free induced pluripotent stem cell-derived neural progenitor cells for in vivo applications. *J Transl Med* 2022; 20: 421.
31. Weber RZ, Grönnert L, Mulders G, et al. Characterization of the blood brain barrier disruption in the photothrombotic stroke model. *Front Physiol* 2020; 11: 586226.
32. Kraler S, Wenzl FA, Georgiopoulos G, et al. Soluble lectin-like oxidized low-density lipoprotein receptor-1 predicts premature death in acute coronary syndromes. *Eur Heart J* 2022; 43: 1849–1860.
33. Lötvall J, Hill AF, Hochberg F, et al. Minimal experimental requirements for definition of extracellular vesicles and their functions: a position statement from the international society for extracellular vesicles. *J Extracell Vesicles* 2014; 3: 26913–26916.
34. Soo CY, Song Y, Zheng Y, et al. Nanoparticle tracking analysis monitors microvesicle and exosome secretion from immune cells. *Immunology* 2012; 136: 192–197.
35. Gardiner C, Ferreira YJ, Dragovic RA, et al. Extracellular vesicle sizing and enumeration by nanoparticle tracking analysis. *J Extracellular Vesicles* 2013; 15: 2.
36. Vestad B, Llorente A, Neurauter A, et al. Size and concentration analyses of extracellular vesicles by nanoparticle tracking analysis: a variation study. *J Extracell Vesicles* 2017; 6: 1344087.
37. Satoh J-I, Onoue H, Arima K, et al. Nogo-A and nogo receptor expression in demyelinating lesions of



- multiple sclerosis. *J Neuropathol Exp Neurol* 2005; 64: 129–138.
38. GrandPré T, Nakamura F, Vartanian T, et al. Identification of the nogo inhibitor of axon regeneration as a reticulon protein. *Nature* 2000; 403: 439–444.
  39. Simonen M, Pedersen V, Weinmann O, et al. Systemic deletion of the myelin-associated outgrowth inhibitor Nogo-A improves regenerative and plastic responses after spinal cord injury. *Neuron* 2003; 38: 201–211.
  40. Cheatwood JL, Emerick AJ, Schwab ME, et al. Nogo-A expression after focal ischemic stroke in the adult rat. *Stroke* 2008; 39: 2091–2098.
  41. Zhang G, Yang L, Kim GS, et al. Critical role of sphingosine-1-phosphate receptor 2 (S1PR2) in acute vascular inflammation. *Blood* 2013; 122: 443–455.
  42. Kim GS, Yang L, Zhang G, et al. Critical role of sphingosine-1-phosphate receptor-2 in the disruption of cerebrovascular integrity in experimental stroke. *Nat Commun* 2015; 6: 7893.
  43. Walter FR, Gilpin TE, Herbath M, et al. A novel in vitro mouse model to study *Mycobacterium tuberculosis* dissemination across brain vessels: a combination of mouse granuloma and blood-brain barrier model. *Curr Protoc Immunol* 2020; 130: e101.
  44. Gaillard PJ and de Boer AG. Relationship between permeability status of the blood-brain barrier and in vitro permeability coefficient of a drug. *Eur J Pharm Sci* 2000; 12: 95–102.
  45. Voeltz GK, Prinz W. a, Shibata Y, et al. A class of membrane proteins shaping the tubular endoplasmic reticulum. *Cell* 2006; 124: 573–586.
  46. Langhorst MF, Reuter A and Stuermer CAO. Scaffolding microdomains and beyond: the function of reggie/flotillin proteins. *Cell Mol Life Sci* 2005; 62: 2228–2240.
  47. Trajkovic K, Hsu C, Chiantia S, et al. Ceramide triggers budding of exosome vesicles into multivesicular endosomes. *Science* 2008; 319: 1244–1247.
  48. Baietti MF, Zhang Z, Mortier E, et al. Syndecan–syntenin–ALIX regulates the biogenesis of exosomes. *Nat Cell Biol* 2012; 14: 677–685.
  49. Willms E, Johansson HJ, Mäger I, et al. Cells release subpopulations of exosomes with distinct molecular and biological properties. *Sci Rep* 2016; 6: 22519.
  50. Vyas N, Walvekar A, Tate D, et al. Vertebrate hedgehog is secreted on two types of extracellular vesicles with different signaling properties. *Sci Rep* 2014; 4: 7357.
  51. Kowal J, Arras G, Colombo M, et al. Proteomic comparison defines novel markers to characterize heterogeneous populations of extracellular vesicle subtypes. *Proc Natl Acad Sci U S A* 2016; 113: E968–77.
  52. Fournier AE, Grandpre T and Strittmatter SM. Identification of a receptor mediating nogo-66 inhibition of axonal regeneration. *Nature* 2001; 409: 341–346.
  53. Davis S, Gale NW, Aldrich TH, et al. Ligands for EPH-related receptor tyrosine kinases that require membrane attachment or clustering for activity. *Science* 1994; 266: 816–819.
  54. Schaupp A, Sabet O, Dudanova I, et al. The composition of EphB2 clusters determines the strength in the cellular repulsion response. *J Cell Biol* 2014; 204: 409–422.
  55. Atapattu L, Lackmann M and Janes PW. The role of proteases in regulating eph/ephrin signaling the role of proteases in regulating eph/ephrin signaling. 2014; 8: 37–41.
  56. Gong J, Körner R, Gaitanos L, et al. Exosomes mediate cell contact-independent ephrin-Eph signaling during axon guidance. *J Cell Biol* 2016; 214: 35–44.
  57. Tassew NG, Charish J, Shabanzadeh AP, et al. Exosomes mediate mobilization of autocrine Wnt10b to promote axonal regeneration in the injured CNS. *Cell Rep* 2017; 20: 99–111.
  58. Simats A and Liesz A. Systemic inflammation after stroke: implications for post-stroke comorbidities. *EMBO Mol Med* 2022; 14: e16269.
  59. Offner H, Subramanian S, Parker SM, et al. Experimental stroke induces massive, rapid activation of the peripheral immune system. *J Cereb Blood Flow Metab* 2006; 26: 654–665.
  60. Esposito E, Ahn BJ, Shi J, et al. Brain-to-cervical lymph node signaling after stroke. *Nat Commun* 2019; 10: 5306.
  61. Paria BC, Vogel SM, Ahmmed GU, et al. Tumor necrosis factor-alpha-induced TRPC1 expression amplifies store-operated Ca<sup>2+</sup> influx and endothelial permeability. *Am J Physiol Lung Cell Mol Physiol* 2004; 287: L1303–1313.
  62. Nwariaku FE, Rothenbach P, Liu Z, et al. Rho inhibition decreases TNF-induced endothelial MAPK activation and monolayer permeability. *J Appl Physiol (1985)* 2003; 95: 1889–1895.
  63. Stanley D, Mason LJ, Mackin KE, et al. Translocation and dissemination of commensal bacteria in post-stroke infection. *Nat Med* 2016; 22: 1277–1284.
  64. Austin V, Ku JM, Miller AA, et al. Ischaemic stroke in mice induces lung inflammation but not acute lung injury. *Sci Rep* 2019; 9: 3622.
  65. Deli MA, Abrahám CS, Kataoka Y, et al. Permeability studies on in vitro blood-brain barrier models: physiology, pathology, and pharmacology. *Cell Mol Neurobiol* 2005; 25: 59–127.
  66. Wahl AS, Omlor W, Rubio JC, et al. Neuronal repair. Asynchronous therapy restores motor control by rewiring of the rat corticospinal tract after stroke. *Science* 2014; 344: 1250–1255.
  67. Lindau NT, Bänninger BJ, Gullo M, et al. Rewiring of the corticospinal tract in the adult rat after unilateral stroke and anti-Nogo-A therapy. *Brain* 2014; 137: 739–756.